Science and Technology of Archaeological Research

Research Article

Studying a Funerary Roman Vessel Glass Collection from Patras, Greece: An Interdisciplinary Characterisation and Use Study

E. Palamara[1]*, N. Zacharias[1], L. Papakosta[2], D. Palles[3], E.I. Kamitsos[3], and J. Pérez-Arantegui[4]

[1]Laboratory of Archaeometry, Department of History, Archaeology and Cultural Resources Management, University of the Peloponnese, 24100 Kalamata, Greece

[2]Ephorate of Antiquities of Achaia, Ministry of Culture, Education and Religious Affairs, 26110 Patras, Greece

[3]Theoretical and Physical Chemistry Institute, National Hellenic Research Foundation, 11635 Athens

[4]Instituto Universitario de investigación en Ciencias Ambientales de Aragó (IUCA), Departamento de Química Analítica, Facultad de Ciencias, Universidad de Zaragoza, 50009 Zaragoza, Spain

Abstract In a rescue excavation of a Roman funerary complex located at the city of Patras, Achaia, Greece, an assemblage of high quality glass vessels of the 2nd-3rd c. AD was recovered. Here we present the results from the physicochemical examination of the collection using a combination of non-destructive techniques, namely optical microscopy, portable X-Ray Fluorescence, Scanning Electron Microscopy and Infrared spectroscopy (IR) techniques. The analyses resulted in the chemical characterization of the glass samples and the identification of a rare example of soda plant-ash glass. Moreover, madder lake was identified as the original content of several glass vessels. Finally, the effect of the original content on the corrosion processes was investigated, along with issues of biocorrosion.

Statement of significance The interdisciplinary study of an assemblage of 2nd-3rd c. AD Roman funerary vessel glasses from Patras, Greece is reported. The archaeological and archaeometric study of Roman glass in south and central Greece has so far been limited. The present work is the first attempt to examine the complete chaîne opératoire of Roman funerary glass vessels, using a multi-technique approach. More specifically, the basic aims of the study were (1) the chemical characterization of the glass and the determination of the raw materials used; (2) the determination of the original content of the vessels; and (3) the examination of the corrosion effects on the glass.

Keywords Roman glass; Patras; plant-ash; madder lake; corrosion

Received 1 October 2015; **accepted** 13 September 2016

Introduction

The city of Patras, located in the northwest Peloponnese, Greece, underwent a period of intense expansion and growth during the 2nd c. AD. Among other valuable objects, funerary findings of the 2nd and 3rd c. AD also include a large number of luxurious glass items, which have so far received limited attention both from an archaeological and an archaeometric point of view (Kolonas 2002). A workshop with 2 furnaces suitable for glassworking has been discovered in the area of Psilalonion, which showed evidence of constant use throughout the Roman period (Papageorgiou 2014). The assumption of local glassworking is further supported by the presence of glass wastes and glass making tools (Triantafyllidis 2006; Triantafyllidis 2007). Furthermore, it is generally considered probable by the excavators and the archaeological community of Patras that, apart from glassworking, there was also a local glass production industry, though no glassmaking workshop has been identified so far. Additionally, importation of glass was still conducted on a large scale, originating either from Mesopotamia or Italy (Liritzis et al. 1997).

Materials and methods

During a rescue excavation at the city centre of Patras a part of the northern Roman cemetery of the city was revealed, which includes a burial building and five roof tiled graves at its north. The graves have been dated to the 2nd-3rd c. AD. Inside one of the graves a group of

*Corresponding author, email: el.palamara@gmail.com

Figure 1 The glass assemblage as recovered forming a pile during the excavation (left) and after the conservation process (right).

vessels was recovered stored originally in a wooden chest, as suggested by the nails that were found close by (Archaiologicon Deltion, in press). Seventeen of the vessels were made of glass and most of them remained intact, together with copper items, possibly children toys (Figure 1). The conservation treatment of the glass vessels is still ongoing. All glass items are of high quality; some of them are considered unique in the area because of their rare form and will be thoroughly studied in the future from an archaeological point of view, after the completion of their conservation.

For the present study, 16 complete glass items and 11 glass fragments were selected. Among the selected samples, the most luxurious and unique vessels as well as characteristic examples of the common classes were included. All vessels have very thin walls, usually 2 to 3 mm. The fragments are even thinner, with a maximum width of 1.2 mm. The majority of the samples are colourless and transparent, usually with a slight blue/green tint. Coloured samples are transparent or translucent and present blue, green, yellow and purple hues.

Optical microscopy using a fibre optics system (FOM/i-scope, Moritex) was performed on all samples, both the complete vessels and the glass fragments, aiming at an initial documentation of their preservation state. Non-destructive, on site portable X-Ray Fluorescence (p-XRF) analysis was applied on all samples using a portable Bruker Tracer III SD set up, with a beam diameter of 3 mm; data quantification was made using S1PXRF software and a custom-built calibration curve, created in collaboration with the scientific personnel of Bruker. The calibration curve was based on the existing file for ceramics, which was then updated based on the measurements of glass standards (1412, NIST610, NIST612, NIST620) through fundamental parameters. In order to optimise the analytical range, two settings were used: (1) an unfiltered low-energy excitation mode (high voltage set at 15 kV and current of 24 μA) was used for the analysis of major and minor elements with an atomic number, Z, between 11 and 29; and (2) an Al/Ti filtered (0.012 inches Al plus 0.001 inches Ti) high-energy excitation mode (high voltage set at 40 kV and current of 12 μA) was used for the analysis of minor and trace elements with an atomic number $Z > 29$. The vessels had been cleaned prior to the analysis, however in most cases their surface exhibited heavy corrosion. At least two measurements were taken for each vessel; the collection time of each measurement was 300 sec.

The limitations of p-XRF in the analysis of archaeological glass have been well documented, the most important being: (1) difficulty in measuring light elements; (2) presence of corrosion layers; (3) thickness of the sample; and (4) geometry of the sample (Liritzis and Zacharias 2011). In order to overcome these problems, the light element analyses were carried out under vacuum. Moreover, care was taken, based on the results of the FOM examination, to select areas with clear glass, flat surface and thick walls.

Due to the corrosion and geometry issues affecting the analyses of the complete vessels, fresh cuts of the 11 glass fragments were also measured by Scanning Electron Microscopy coupled with an Energy Dispersive Spectrometer (SEM/EDS). Microsamples were cut off, embedded in resin and polished. The polished samples were analyzed under a SEM type JEOL JSM-6510LV coupled with an Oxford Instruments EDS. The analytical data were obtained by INKA software. The bulk analyses were conducted at high vacuum, 20 kV accelerating voltage and with a count time of 300 sec. Each sample was measured at least five times.

The accuracy of the quantitative procedure was evaluated using the following certified reference glasses: 1412, NIST610, NIST612 and NIST620. The

results for the SEM/EDS show an overall very good agreement with the certified values (Table 1).

The XRF data were estimated twice: (1) calculating the composition of all major elements ("XRF" column); and (2) without calculating the Na_2O values ("XRF*" column). The XRF data are more problematic, demonstrating wide variations especially for CaO. When the Na_2O values are disregarded there is a slightly improved accuracy of most elements and especially SiO_2, which is expected given the known limitations of XRF analysis of light elements.

The analysis and process of additional glass standards covering a wider compositional range is currently under way in order to improve the accuracy of the calibration curve. The presently available XRF analytical data was used in two ways: (1) for the qualitative identification of minor elements used as colourants or decolourizers (Fe, Mn, Co, Cu, Sb); and (2) for the comparison of the composition of the samples within the assemblage, and more specifically of the fragments also analysed by SEM/EDS with the complete vessels, which could not be analysed with other techniques.

In addition to the analytical techniques, Infrared spectroscopy (IR) was applied in order to characterize the glass matrix and examine the corrosion patterns visible on the glass fragments. IR spectra were obtained by a Hyperion infrared microscope; the spectra were measured in the reflectance mode in the range of 370–7000 cm^{-1}. Each spectra represents the average of 128 scans. More detailed information on the methodology applied for the analysis of the spectra is presented by Möncke et al. (2013).

Finally, Laser Desorption –Ionization – Time of Flight – Mass Spectrometry (LDI-ToF-MS) was applied for the identification of residues. More detailed information on the use of this analytical technique is presented by Pérez-Arantegui et al. (2009). In LDI-MS, the sample is directly placed in a metallic target plate, in our case just some drops (0.5 μl) of ethanol with some particles in suspension, then the solid is ionized by the action of a laser (a 337-nm pulsed nitrogen UV laser (20 Hz)). The resulting ions are transported to the mass analyzer, with an accelerating voltage of 19 kV. In our case, desorption and ionization of the sample was performed directly (LDI) without the assistance of a matrix.

Chemical characterization

The chemical composition of the glass fragments as determined by SEM/EDS is presented in Table 2. The additional use of p-XRF was necessary in order to conduct the *in situ* chemical analysis of the complete vessels, which could not be moved or sampled. However, the corrosion layers present on the samples, in addition to the well-known analytical limitations of the technique, lead to a significant underestimation of the sodium content (in most cases below 5 wt%). In order to overcome this problem, Zacharias et al. (2008) suggest the replacement of the sodium and magnesium value by a value calculated by a different technique, or by using an estimate value from published data of similar glasses with those under study. The remaining percentage is then distributed to all remaining components on the basis of their relative XRF values.

In this case, it was decided to replace only the sodium values, since the accuracy of the calculation of magnesium is good, for MgO concentrations close to those expected for roman glasses. Moreover, MgO is not expected to be highly affected by corrosion effects. Regarding sodium, and given the limited availability of related published data and the good accuracy of the SEM data, we used an estimation based on the SEM measurements. A mean value of Na_2O concentration (19.01 wt%) was estimated from the SEM/EDS analysis of the fresh cuts and then assigned to all samples. The XRF values that occurred for the major oxides of each sample, after re-normalizing to 100%, are presented in Table 3.

The comparison of the p-XRF data for the in situ measurements of the complete vessels and the glass fragments verifies that all the samples of the assemblage share similar compositional characteristics (Figure 2). Some variations noted between the vessels and the fragments can be attributed to geometry issues, taking into consideration that most fragments had much thinner walls than the restored items. The larger variations are noted for calcium, which has generally lower values for the fragments.

All samples of the assemblage belong to the general type of soda-lime-silica glass; the alkali source used is natron. One sample (sample G41OM28) demonstrates a significantly diverse composition and will be discussed separately below.

Manganese is the most common decolourizer used during the Roman period, especially for the colourless glasses with a Syrian origin (Jackson 2005). The same trend is noticed among the 16 colourless samples of the present assemblage, which have a manganese concentration of approximately ca 0.5 wt%, whereas antimony is either completely absent (Figure 3a), or occasionally identified in trace amounts.

Dark blue colour is attributed to small quantities of cobalt (<0.2 wt %), though copper is also found in equal quantities (Figure 3b). In one of the dark blue samples (G31OM16a), cobalt was below the SEM/EDS detection limit, it was however identified with XRF. Light blue and emerald green objects are coloured with the use of copper, at concentrations of ~1 wt% and ~0.4 wt% respectively (Figure 3c). The purple samples show high concentrations of manganese oxides (~2.8 wt %) (Figure 3d). Finally, the only colouring agent detected on the yellow vessel is iron oxide, in a concentration of ca 1 wt% (Figure 3e). Similar examples of the use of iron as a colourant on yellow roman glasses have been previously described in other studies (Gedzevičiūtė et al. 2009).

Table 1 Certified values and the XRF and SEM/EDS results of the analysed glass samples (1412, NIST610, NIST612 and NIST620) (oxides in weight %, normalised to 100%; relative error presented as percentage %; "nd": non detected).

	1412				610				612				620			
	Certified values	XRF	XRF*	SEM	Certified values	XRF	XRF*	SEM	Certified values	XRF	XRF*	SEM	Certified values	XRF	XRF*	SEM
Na_2O (wt%)	6.90	9.67	-	7.42	13.96	14.53	-	14.43	14.00	16.01	-	13.03	14.42	19.00	-	14.58
Relative error (%)	1.5	35.6	-	9.8	Not available	24.7	-	1.8	Not available	23.0	-	1.5	0.4	23.8	-	2.0
MgO (wt%)	6.90	2.28	2.95	6.82									3.70	3.30	3.49	3.73
Relative error (%)	Not available	8.6	8.6	13.2									1.4	4.9	4.9	5.7
Al_2O_3 (wt%)	11.06	12.96	13.26	11.99	1.99	2.13	2.14	1.84	2.00	1.74	1.78	2.12	1.80	1.66	1.75	1.72
Relative error (%)	3.2	2.1	2.1	13.9	Not available	0.8	0.8	8.2	Not available	0.3	0.3	8.5	1.7	0.5	0.5	9.5
SiO_2 (wt%)	62.34	59.21	60.62	61.80	71.81	66.75	67.19	71.85	71.98	65.63	67.20	73.43	72.21	65.44	69.14	72.72
Relative error (%)	0.4	1.9	1.9	3.5	Not available	1.4	1.4	0.7	Not available	1.2	1.2	0.8	0.1	1.3	1.3	0.8
SO_3 (wt%)													0.28	0.46	0.48	0.35
Relative error (%)													7.1	6.4	6.1	20.0
K_2O (wt%)	6.09	8.98	9.19	6.13	0.05	0.01	0.01	nd	0.01	nd	nd	nd	0.41	0.31	0.33	0.40
Relative error (%)	2.4	0.9	0.9	24.3	Not available	50.0	50.0	-	Not available	-	-	-	7.3	6.1	5.7	20.0
CaO (wt%)	6.66	6.63	6.79	5.85	11.97	16.28	16.39	11.88	12.00	16.36	16.75	11.43	7.12	9.54	10.08	6.50
Relative error (%)	2.2	0.7	0.7	13.0	Not available	1.4	1.4	2.1	Not available	1.6	1.6	2.0	0.7	1.9	1.8	2.6
TiO_2 (wt%)					0.044	0.071	0.072	nd	0.005	nd	nd	nd	0.018	nd	nd	nd
Relative error (%)					Not available	4.4	4.3	-	1.6	-	-	-	11.1	-	-	-
MnO (wt%)					0.048	0.102	0.103	nd	0.004	0.038	0.039	nd				
Relative error (%)					2.1	2.6	2.6	-	2.0	0.5	0.5	-				
Fe_2O_3 (wt%)	0.046	0.282	0.289	nd	0.046	nd	nd	nd	0.005	0.196	0.200	nd	0.043	0.287	0.303	nd
Relative error (%)	Not available	0.2	0.2	-	2.0	-	-	-	3.9	9.6	9.5	-	9.3	8.4	7.9	-
CoO (wt%)					0.039	0.054	0.055	nd	0.004	0.010	0.011	nd				
Relative error (%)					Not available	1.1	1.1	-	3.4	4.0	3.6	-				
CuO (wt%)					0.044	0.071	0.071	nd	0.004	0.014	0.014	nd				
Relative error (%)					0.9	1.1	1.1	-	2.4	3.6	3.6	-				

STAR2016205489 23.2016.1239868

Table 2 SEM-EDS compositional analysis of the glass fragments (oxides in weight %, normalised to 100%; "nd": non detected).

Sample	Colour	Na_2O	MgO	Al_2O_3	SiO_2	P_2O_5	Cl	K_2O	CaO	MnO	Fe_2O_3	CoO	CuO
G31OM16	Colourless	19.46	0.48	2.21	69.63	nd	1.04	0.56	6.30	0.16	0.16	nd	nd
G31OM16b	Colourless	19.93	0.80	2.25	68.09	nd	1.08	0.44	6.47	0.63	0.31	nd	nd
G31OM16c	Colourless	19.67	0.39	2.62	70.44	nd	0.95	0.44	5.34	0.15	nd	nd	nd
G34OM16	Colourless	19.18	0.41	2.48	69.53	nd	1.04	0.55	6.11	0.27	0.46	nd	nd
G35OM16	Colourless	19.58	0.44	2.39	69.20	nd	1.18	0.35	6.09	0.52	0.25	nd	nd
Ryto	Colourless/purple	20.29	0.48	2.51	68.74	nd	1.21	0.56	5.58	0.34	0.28	nd	nd
G12OM11	Purple	17.62	0.45	2.20	69.27	nd	1.03	0.63	7.16	1.16	0.49	nd	nd
G41OM28	Light green	20.21	4.23	2.08	63.59	1.20	0.72	1.33	5.05	0.78	0.80	nd	nd
G43OM32	Light blue	19.11	0.42	2.31	67.96	0.00	0.91	0.87	6.64	0.46	0.27	nd	1.04
G31OM16a	Dark blue	17.55	0.51	2.57	71.77	0.00	1.01	0.49	5.69	0.00	0.34	nd	0.07
G33OM16	Dark blue	16.54	0.49	2.60	70.71	0.00	0.22	0.45	6.60	0.12	0.93	0.63	0.72

It is generally accepted that Roman glasses were manufactured in large centres located around the eastern Mediterranean. The glass ingots formed were then traded to many secondary centres (Jackson and Cottam 2015). However, the so far available information on the organization of Roman glassmaking and glassworking between the 1st and 3rd c. AD is limited. Reference groups are usually described in terms of colour, and more specifically by the presence of specific colourants and decolourizers, while colourless and naturally coloured glasses have been more thoroughly studied than coloured glasses (Mirti et al. 1993; Silvestri et al. 2005).

Figure 4 presents Al_2O_3 versus CaO concentrations for the samples of the present assemblage, calculated by SEM/EDS, along with previously published data of 1st-3rd c. AD glasses from Patras (Liritzis et al. 1997), Binchester, Lincoln and Colchester in Britain (Paynter 2006) and 9 other areas across the Roman Empire, namely Jordan (Petra and Barsinia), Georgia (Gonio), Italy (Iulia Felix and Embiez shipwrecks, Augusta Praetoria), Spain (Barcino) and Belgium (Tienen and Oudenburg) (Ganio et al. 2012). The majority of these assemblages was analyzed by SEM/EDS, with the exception of the glasses from Iulia Felix shipwreck (XRF), from Tienen (Atomic Emission Spectrometry) and finally from the Embiez shipwreck and Augusta Praetoria (ICP-OES). Therefore, the data shown in Figure 4 was acquired by surface techniques apart from the two cases in which ICP-OES was carried out.

A correlation of the two oxides is evident, though the sample distribution is only partly correlated to the excavation site. The samples from Patras form a cluster with low alumina and calcium values. The lower part of the plot is generally accepted to consist of antimony-decoloured glasses, such as the Iulia Felix, Binchester, Lincoln and Colchester samples, which is not the case for the Patras samples. However, the presently studied samples correlate well with previously studied glasses from Patras, which were again decolourized by the addition of manganese (Liritzis et al. 1997). The thorough analysis of the trace elements present in the body of the glass, which is a future task, could assist in the comparison with similar glasses recovered in other sites.

Plant ash flux

Sayre and Smith (1961) demonstrated the existence of two principal groups of ancient soda-lime-silica glass: (1) A low-magnesia, low-potash glass group, with K_2O and MgO each below about 1.5 wt%, which is characterized by the use of mineral soda (natron) as the alkali source, and (2) a high-magnesia, high-potash glass group, with K_2O and MgO in excess of 1.5 wt%, in which a soda plant-ash is added. The former group is characteristic of the Roman world and was the dominant glass type from the middle of the 1st millennium BC until the 9th century AD. The latter group is found throughout the Near East before the 7th century BC and, after a long period of absence, reappears in the Islamic world after the 9th century AD and in Europe from the 12th century AD.

Sample G41OM28 demonstrates a unique composition among the glasses of the present assemblage (Table 2). The sample is translucent and light green in colour. Contrary to the other green samples of the assemblage, no copper is detected and the colour is attributed to the increased presence of iron oxides. It has relatively high amounts of K_2O, in addition to high amounts of Na_2O, which indicates the use of soda plant-ash. The presence of P_2O_5 and the increased concentration of MgO serve as additional indications of the presence of a plant-ash component, which is unusual for Roman glass of the 2nd – 3rd c. AD.

Other examples of early Roman glass with plant-ash flux have previously been identified in small numbers throughout Europe. The vast majority of these examples are either emerald green or red, coloured with the addition of copper (Paynter and Dungworth 2011; Jackson and Cottam 2015). In addition to the common colour, Jackson and Cottam (2015) demonstrated that the use of emerald green plant-ash glass was restricted to the production of specific types of vessels. Fewer plant-ash glasses of the same period with blue and black colour, as well as green samples without copper have also been identified (Van der Linden et al. 2009; Gallo et al. 2013).

In the area of Patras three more plant-ash glasses have been previously identified among Roman

STAR2016205489 23.2016.1239868

Table 3 XRF compositional analysis of the glass fragments and the complete vessels (mean values and standard deviations of two analyses per sample, oxides in weight %, normalised to 100%, "nd": not detected). A mean Na_2O value (19.01 wt %) was calculated by SEM/EDS for all samples.

Sample	Colour	Type		Na_2O	MgO	Al_2O_3	SiO_2	P_2O_5	SO3	K_2O	CaO	TiO_2	MnO	Fe_2O_3	CoO	CuO
G5OM10	Colourless	Vessel	m	19.01	0.41	2.03	70.97	0.13	0.08	0.37	6.46	0.02	0.31	0.19	nd	0.01
			s	-	0.01	0.04	0.55	0.07	0.12	0.06	0.14	0.01	0.04	0.14	-	
G7OM13	Colourless	Vessel	m	19.01	0.41	2.03	70.95	0.12	0.14	0.29	6.37	0.01	0.12	0.55	nd	nd
			s	-	0.00	0.02	0.11	0.01	0.04	0.03	0.20	0.01	0.01	0.00	-	-
G15OM13	Colourless	Vessel	m	19.01	0.42	2.09	70.03	0.22	0.30	0.36	6.43	0.08	1.06	nd	nd	nd
			s	-	0.01	0.06	1.16	0.12	0.02	0.05	0.61	0.03	0.50	-	-	-
G16OM13	Colourless	Vessel	m	19.01	0.41	2.00	71.30	0.07	0.08	0.25	6.42	0.01	0.29	0.16	nd	nd
			s	-	0.01	0.03	0.38	0.01	0.11	0.01	0.56	0.00	0.03	0.06	-	-
G17OM13	Colourless	Vessel	m	19.01	0.42	2.08	69.97	0.18	0.24	0.45	6.88	0.02	0.74	nd	nd	nd
			s	-	0.01	0.03	0.38	0.01	0.11	0.01	0.56	0.00	0.03	-	-	-
G18OM13	Colourless	Vessel	m	19.01	0.41	2.04	69.65	0.28	0.33	0.32	6.97	0.01	0.99	nd	nd	nd
			s	-	0.01	0.07	0.15	0.07	0.17	0.03	0.17	0.00	0.03	-	-	-
G19OM13	Colourless	Vessel	m	19.01	0.41	2.04	70.01	0.28	0.44	0.38	6.96	0.02	0.44	0.01	nd	nd
			s	-	0.00	0.02	0.90	0.16	0.20	0.02	0.40	0.01	0.08	0.01	-	-
G21OM13	Colourless	Vessel	m	19.01	0.41	1.99	71.00	0.11	0.21	0.31	6.39	0.04	0.44	0.09	nd	nd
			s	-	0.00	0.02	0.75	0.01	0.09	0.09	0.98	0.02	0.10	0.07	-	-
G24OM13	Colourless	Vessel	m	19.01	0.41	2.00	70.08	0.17	0.54	0.28	6.29	0.01	1.21	nd	nd	nd
			s	-	0.01	0.04	1.40	0.15	0.09	0.02	0.69	0.01	0.40	-	-	-
G25OM13a	Colourless	Vessel	m	19.01	0.42	2.06	71.14	0.22	0.16	0.18	6.29	0.01	0.18	0.34	nd	nd
			s	-	0.00	0.00	0.06	0.01	0.03	0.01	0.01	0.00	0.01	0.03	-	-
G25OM13b	Colourless	Vessel	m	19.01	0.40	1.99	71.65	0.12	0.09	0.36	5.57	0.01	0.04	0.77	nd	nd
			s	-	0.00	0.00	0.56	0.04	0.01	0.08	0.39	0.01	0.011	0.04	-	-
G31OM16	Colourless	Fragment	m	19.01	0.44	2.18	70.46	0.39	0.46	0.36	5.87	0.05	0.27	0.53	nd	nd
			s	-	0.01	0.07	0.23	0.33	0.25	0.34	0.04	0.04	0.08	0.14	-	-
G31OM16b	Colourless	Fragment	m	19.01	0.44	2.17	71.59	0.01	0.00	0.26	6.08	0.03	0.27	0.14	nd	nd
			s	-	0.02	0.08	0.25	0.01	0.00	0.02	0.59	0.01	0.27	0.10	-	-
G31OM16c	Colourless	Fragment	m	19.01	0.42	2.06	71.23	0.28	0.86	0.22	5.25	0.02	0.65	nd	nd	nd
			s	-	0.01	0.04	0.83	0.06	0.73	0.10	0.25	0.01	0.12	-	-	-
G34OM16	Colourless	Fragment	m	19.01	0.43	2.12	72.18	0.10	0.07	0.32	5.27	0.01	0.20	0.29	nd	nd
			s	-	0.01	0.04	0.67	0.13	0.05	0.07	0.02	0.00	0.32	0.21	-	-
G35OM16	Colourless	Fragment	m	19.01	0.41	2.00	72.31	0.07	0.05	0.18	5.38	0.01	0.57	nd	nd	nd
			s	-	0.01	0.04	0.76	0.14	0.02	0.03	0.09	0.00	0.05	-	-	-
G43OM32	Light Blue	Vessel	m	19.01	0.40	1.95	72.42	0.00	nd	0.31	5.39	0.03	0.44	nd	0.02	0.04
			s	-	0.00	0.01	0.09	0.00	-	0.02	0.07	0.00	0.00	-	0.00	0.00
G43OM32	Light Blue	Fragment	m	19.01	0.43	2.10	69.64	0.27	0.90	0.46	5.67	0.02	1.20	nd	nd	0.30
			s	-	0.02	0.11	1.96	0.19	0.64	0.11	0.20	0.01	0.54	-	-	0.19
G31OM16a	Dark Blue	Fragment	m	19.01	0.45	2.20	70.51	0.27	0.07	0.35	6.81	0.02	0.25	nd	0.03	0.03
			s	-	0.01	0.07	0.61	0.00	0.10	0.08	0.81	0.00	0.67	-	0.02	0.00
G33OM16	Dark Blue	Fragment	m	19.01	0.44	2.16	70.98	0.06	nd	0.33	6.45	0.02	0.35	nd	0.12	0.08
			s	-	0.01	0.03	0.33	0.15	-	0.01	0.25	0.00	0.07	-	0.07	0.04

G13OM11	Emerald	Vessel	m	19.01	0.42	2.09	67.55	0.38	1.15	0.46	7.49	0.02	0.54	0.55	nd	0.35
			s	-	0.00	0.01	0.55	0.01	0.24	0.06	0.04	0.01	0.33	0.46	-	0.00
G41OM28	Light green	Vessel	m	19.01	3.63	1.78	62.97	1.49	nd	1.49	6.25	0.09	3.30	nd	nd	nd
			s	-	0.07	0.04	0.61	0.07	-	0.06	0.26	0.00	0.11	-	-	-
G41OM28	Light green	Fragment	m	19.01	3.56	1.75	65.90	0.72	nd	0.96	5.47	0.08	2.55	nd	nd	nd
			s	-	0.04	0.02	2.92	0.24	-	0.62	0.58	0.01	0.84	-	-	-
G12OM11	Purple	Vessel	m	19.01	0.42	2.04	68.64	0.10	nd	0.58	6.37	0.02	2.82	nd	nd	nd
			s	-	0.01	0.04	0.55	0.04	-	0.04	0.47	0.00	0.13	-	-	-
G12OM11	Purple	Fragment	m	19.01	0.43	2.09	69.42	0.16	nd	0.52	5.72	0.03	2.64	nd	nd	nd
			s	-	0.02	0.11	1.42	0.04	-	0.10	0.34	0.00	1.38	-	-	-
Ryto	Colourless/Purple	Fragment	m	19.01	0.46	2.25	66.66	0.18	0.02	0.39	5.89	0.03	5.11	nd	nd	nd
			s	-	0.02	0.11	1.95	0.02	0.01	0.09	0.13	0.00	1.75	-	-	-
G26OM13	Yellow	Vessel	m	19.01	0.41	2.00	71.67	0.08	0.50	0.19	5.23	0.03	0.02	0.87	nd	nd
			s	-	0.01	0.04	0.16	0.02	0.16	0.02	0.14	0.01	0.00	0.09	-	-

assemblages of the same period: Papageorgiou (2014) reports two early 2nd c. AD glasses and Liritzis et al. (1997) report one glass among an assemblage of 1st - 2nd c. AD funerary glass vases. These three glasses are green and share significantly similar compositions with that of sample G41OM28. It is important to highlight that these four examples of green plant-ash glass from Patras are coloured by the addition of iron instead of copper, their composition is therefore atypical of the early roman plant-ash glasses found elsewhere.

The model of production and distribution of early plant-ash glasses is still unclear. Liritzis et al. (1997) suggest a near eastern influence, based on the (Na_2O +K_2O)/(CaO+MgO) ratio of the plant-ash glass. The Mesopotamian origin is further corroborated by the reported production of plant-ash glass in the Mesopotamian region under the Sasanian rule (3rd to 7th c. AD) (Mirti et al. 2008). Jackson and Cottam (2015) make a hypothesis for the existence of a set trading framework, resulting in the distribution of emerald green plant-ash glass to a limited number of secondary workshops.

Identification of residues

A residue of an intense pink colour was found attached to the inner surface of a number of colourless samples (Figure 5). The chemical analysis of the residue showed that it is an aluminosilicate substance, with relatively high sulphur content (Table 4). Both the colour of the residue and its chemical composition resemble madder lake, a red lake pigment which was used during the Roman period (Eastaugh et al. 2004) and has previously been identified as a cosmetic residue in Roman glass vessels (Hottentot and Van Lith 2006; Van Elslande et al. 2008; Pérez-Arantegui et al. 2009). This pigment is extracted from the common madder plant, Rubia tinctorum, and it can contain two organic red dyes: alizarin and purpurin. In order to prepare the red pigment, the dyes must be precipitated together with an aluminium-containing compound, i.e. alum or clay, to produce a very fine red powder, suitable for cosmetic use.

In order to reliably identify the residue, Laser Desorption –Ionization – Time of Flight – Mass Spectrometry (LDI-ToF-MS) was applied.

The analysis clearly identified the presence of alizarin as the main component of the organic dye and therefore verified the characterization of the pink residue as a madder lake (Figure 6). The characteristic negative ions at m/z 240 and 239 corresponded to the radical alizarin ion $[A]^{\bullet}$ and the deprotonated alizarin molecule $[A\text{-}H]^{-}$. They would confirm the presence of alizarin or other madder components with a molecular mass of 240 Da. The most intense ion at m/z 225, also highlighted in the madder reference spectra (Pérez-Arantegui et al. 2009), may have

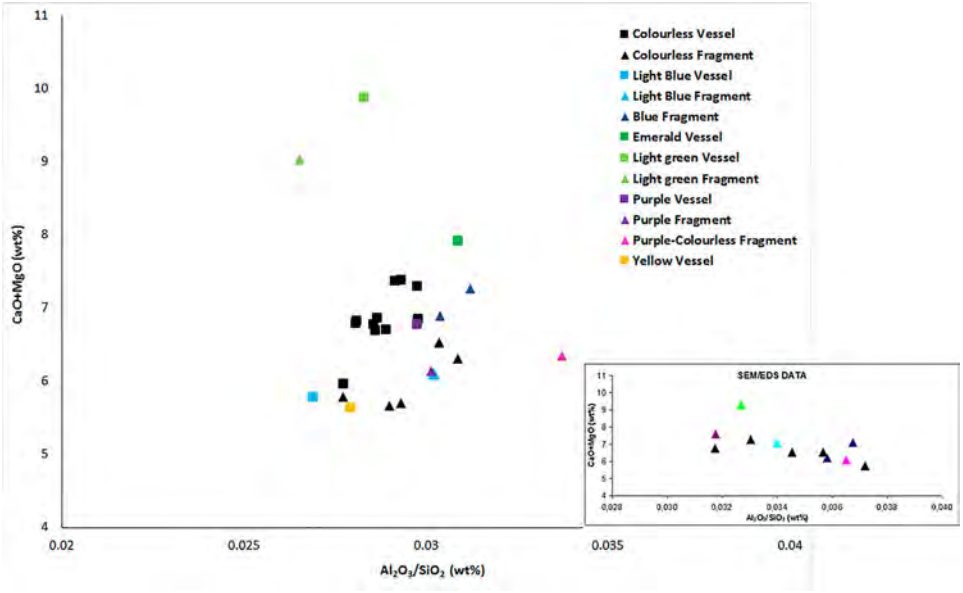

Figure 2 Comparison of the chemical composition of fragments and complete vessels, determined by p-XRF (Inset plot: composition of glass fragments determined by SEM/EDS).

come from a fragmentation of the anthraquinones or from a by-product.

Corrosion effects

Corrosion effects of the plant-ash sample

The plant-ash sample (G41OM28) shows signs of higher degree and different mechanisms of corrosion. The surface of the sample is covered by extensive micropitting (Figure 7). Additionally, two successive corrosion layers have been formed (Figure 8): (1) an iridescent layer, completely depleted in alkalis and metals, with a consequent high increase in silica and alumina; and (2) a browning layer, enriched in metals which are present in the pristine glass in very low amounts, such as Ti, Fe and Mn. Additionally, Pb is identified in this layer, although it is not identified in the pristine glass and no lead object was recovered in the proximity of the glass items (Table 5).

The surface of the browning layer shows signs of intense biological contribution to the corrosion process. Macropitting is evident throughout the browning layer, mostly in formations of concentric circles (Figure 8). SEM/EDS mapping of the composition of one such formation shows the presence of rings with a high silica concentration, succeeded by Mn- and Fe-rich rings (Figure 9).

Glasses with a plant-ash component demonstrate different mechanisms and higher rates of corrosion than soda-lime glasses (Bertoncello et al. 2002; Domenech-Carbo et al. 2006; Tournie et al. 2008). Moreover, Perez y Zorba et al. (1980) suggest that the high concentration of manganese is favourable to the presence of ferrobacteria, while other elements such as copper salts are known to be poisonous to micro-organisms, thus inhibiting biocorrosion. Therefore, slight differences in composition could explain why this particular sample is the only one showing signs of biocorrosion, even though all glass items were stacked together on a pile.

Corrosion effects due to content

A number of vessels showed more intense macroscopic signs of corrosion on the inside surface of their walls than on the outside surface. In order to further investigate the corrosion effects of the samples, IR spectroscopy was applied. IR spectroscopy is often used in the corrosion analysis of both archaeological and modern glasses (Tournié et al. 2008; Lynch et al. 2007). The SiO_4 tetrahedra are present in the glass matrix with different tetrahedral arrangements, each with characteristic IR signatures. Isolated SiO_4 tetrahedra are referred to as Q^0 and tetrahedra with 'n' common bridging oxygen atoms as Q^n. Given the chemical composition of the samples under study, the Q^3 units are expected to be the most common silicate unit in pristine glass, next to a small fraction of Q^2 groups. Depending on the corrosion processes affecting the glass, the formation of either a polymerized or a depolymerized glass network is possible. Polymerization leads to the significant increase of Q^4 units. On the contrary, depolymerisation results in an increased break up of the glass network, which is revealed through the decrease of the Q^3 band and the increase of the Q^1 and Q^2 bands (Möncke et al. 2013).

IR spectra from different areas of several sherds revealed that there is indeed a difference in both the degree and the mechanism of corrosion between the inside and outside surfaces. Figure 10 shows three IR spectra from different areas of the same vessel. The spectrum of the core (black line) represents the healthy part of the glass and shows the typical Q^3 and Q^2 bands for soda-lime-silica glass. In the spectrum of the inside surface (red line) the (Si-O)

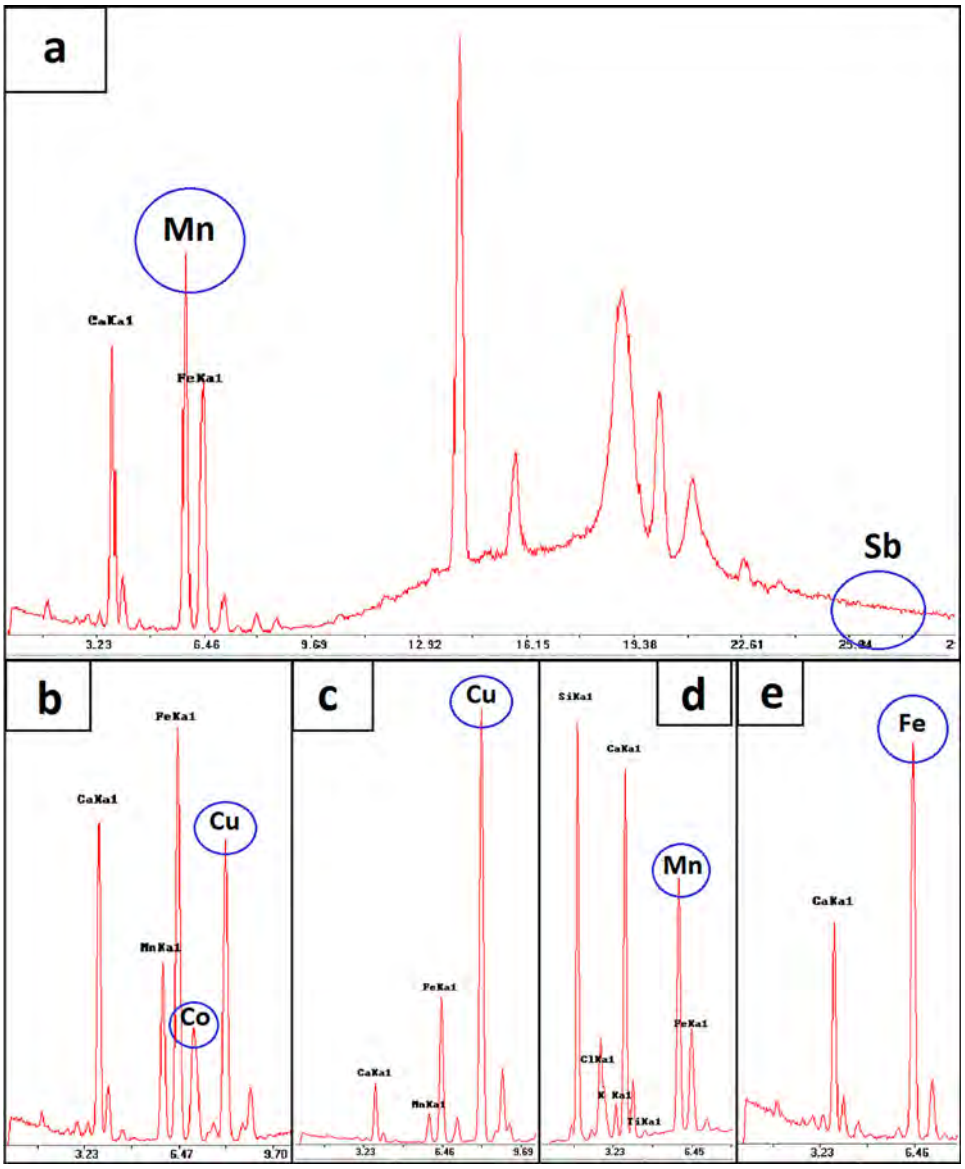

Figure 3 Representative XRF spectra showing the decolourizers (3a) and common colourants for each colour group (3b: Dark blue; 3c: Green and light blue; 3d: Purple; 3e: Yellow).

asymmetric stretching band has shifted towards higher frequencies (at ~1100 cm^{-1}), while the Q^2 band is altogether absent. Both the band at ~1100 cm^{-1} and the appearance of the shoulder at ~1200 cm^{-1} are attributed to the asymmetric stretching vibrations of Si-O-Si bridges in a three dimensional network of Q^4 silicate units. These alterations suggest the formation of a layer of highly polymerized glass on the inside of the vessel walls.

The spectrum of the outside surface (blue line) however, demonstrates a different corrosion pattern: two distinct bands, centered at ~910 cm^{-1} and ~1080 cm^{-1} appear. The first one, which was not visible in the spectrum of the core and appears now strong, can be attributed to Q^1 tetrahedra, indicating increased break up of the glass network. The band centered at ~1080 cm^{-1} is probably a combination of mainly Q^3 tetrahedra with a contribution from the formation of Si-O-Al bonds. It seems therefore, that a depolymerized layer is formed on the outside surface of the walls.

The SEM/EDS compositional analysis corroborates the results of IR spectroscopy. Figure 11 shows a concentration profile of the major elements conducted on a fresh section of a colourless vessel, focusing specifically on two zones of 40 μm on the inside and outside edge of the wall. On the inside surface, a 10 μm polymerized layer is formed, which shows a high loss of alkali and a consequent significant increase in the concentration of silica. Calcium remains stable throughout the corrosion zone, whereas alumina is slightly increased towards the edge. In the contrary, the outside corrosion zone is significantly thinner, approximately 2 μm in width. The decrease in the concentration of silica and the respective increase in alumina suggest a depolymerized network. The sodium and calcium composition remains unaltered.

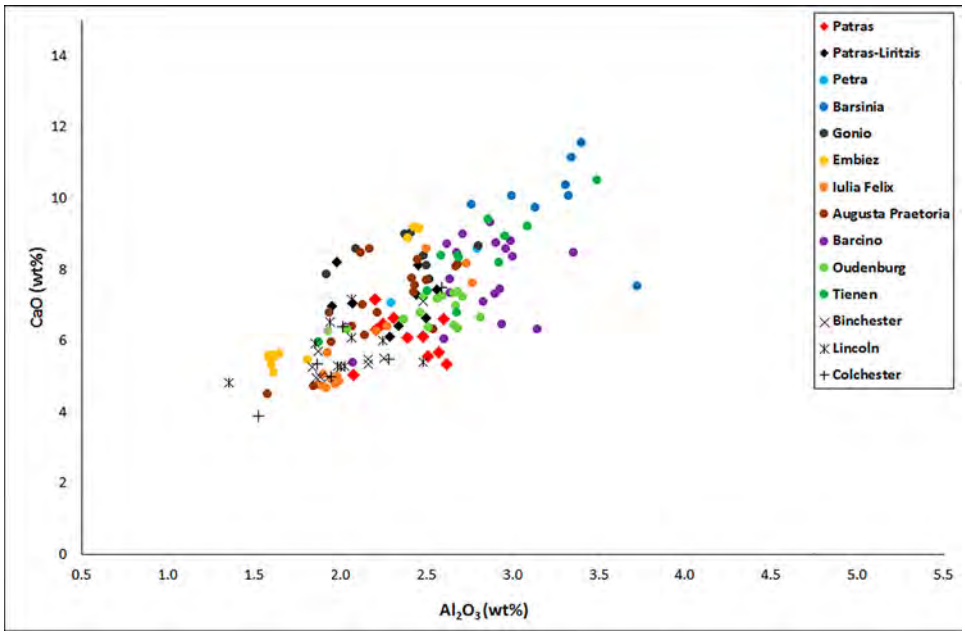

Figure 4 Alumina versus calcium concentration of the studied glasses (red spots – "Patras") along with published data from Patras ("Patras-Liritzis") – presented in Liritzis et al. 1997, Jordan ("Petra" and "Barsinia"), Georgia ("Gonio"), Italy ("Iulia Felix", "Embiez", "Augusta Praetoria"), Spain ("Barcino"), Belgium ("Tienen", "Oudenburg") – presented in Ganio et al. 2012, Britain ("Binchester", "Lincoln", "Colchester") – presented in Paynter 2006.

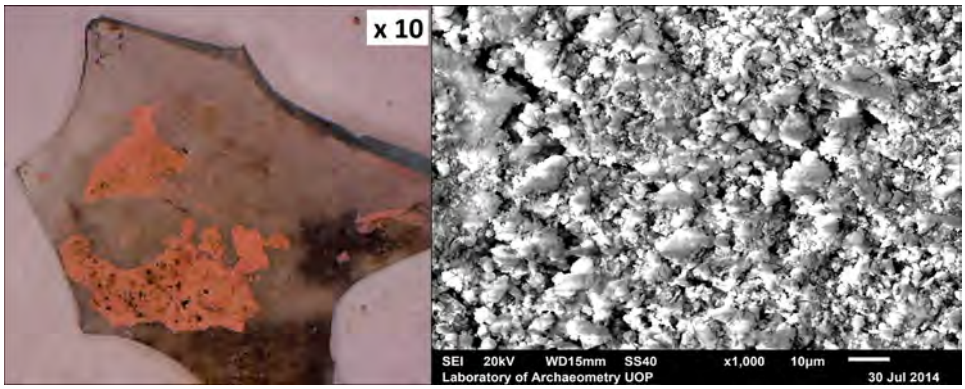

Figure 5 FOM microscope image x10 (Left) and SEM image x1000 (Right) of the pink residue.

Table 4 EDS compositional analysis of the pink residue (weight %, normalised to 100%).

	MgO	Al_2O_3	SiO_2	SO_3	K_2O	CaO	TiO_2	FeO
Pink residue	2.23	45.34	41.74	2.66	1.34	2.64	0.38	3.68

Leaching experiments of alkali-silicate glasses have showed that the exact corrosion process occurring in each case is highly complex and determined by a number of different parameters, more importantly the original composition of the glass and the environment (Tournié et al. 2008). Additionally, the corrosion process is time-dependent, since it has been shown that the initial depolymerisation of the glass can be followed at longer leaching times by the formation of a gel-layer which transforms into a silica type network (Lynch et al. 2007).

Taking into consideration the very small width of the walls we cannot attribute the above mentioned corrosion effects to microtopographic differences. High corrosion effects of the inside surfaces have previously also been reported in relation to the madder lake residue (Zacharias and Palamara 2016). More specifically, thick corrosion zones with significant increase of Al_2O_3 were formed on the inside walls of vessels containing madder lake. Given the available data it is not possible at this point to propose a specific process which would fully account for the corrosion

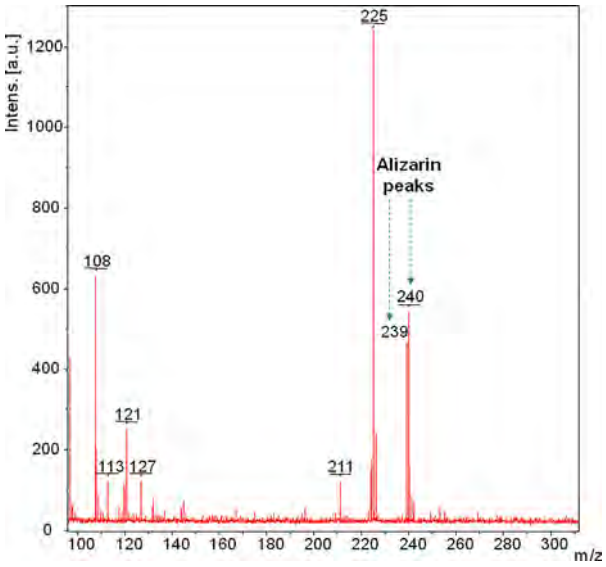

Figure 6 Negative-ion mass spectrum obtained by LDI-ToF-MS in the pink residue.

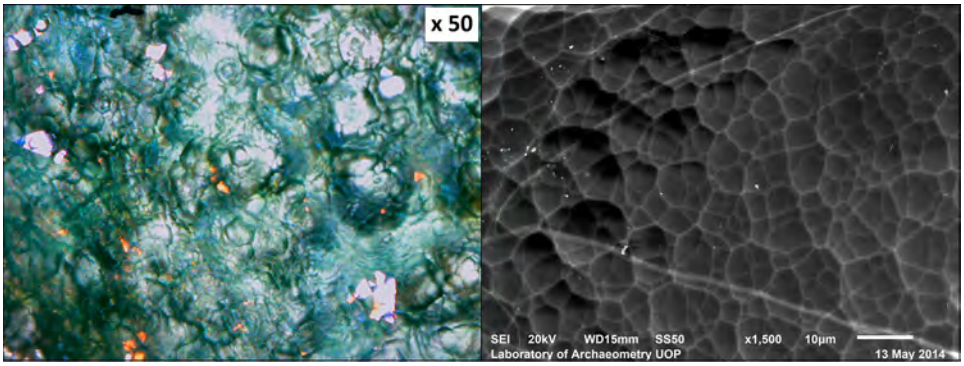

Figure 7 Extensive micropitting on the surface of the plant-ash sample (Left: FOM microscope image x50; Right: SEM image x1500).

effects. However, we suggest that the original content played a critical role in the corrosion effects of the glass samples, even in cases where the vessels broke at some unknown point in the past.

Concluding remarks

A holistic study of an assemblage of funerary glass vessels is reported, combining standard non-invasive and advanced spectroscopic methods to tackle questions of material characterization, corrosion and use of the glass vessels.

The glass samples belong to the soda-lime-silica type and their composition is in good agreement with previously published data of Roman glass assemblages recovered in Patras. The alkali source used is natron. Manganese was used as a decolourising agent in the colourless glasses. The colourants identified are iron oxide (yellow), copper (green, light blue), cobalt (dark blue) and manganese (purple).

One green sample has an atypical composition, as plant-ash is added as the alkali source instead of natron. In comparison with published data, this sample shares the same compositional traits with three other green samples recovered in different tombs in Patras. Plant-ash glasses dating to the Roman period are rare and their model of production and distribution is still unclear.

A pink residue of the original content was identified in a number of samples. The aluminosilicate substance was securely identified as madder lake, a red lake pigment which was often used during the Roman period as a dye or a cosmetic.

A number of different corrosion effects are noted among the samples of the assemblage. The plant-ash sample shows a significantly higher degree of corrosion. It is the only sample in which a silver iridescent and a browning layer have been formed. Biocorrosion also seems to have been an additional weathering factor.

Moreover, the inside surfaces of the walls of some colourless sherds demonstrate high polymerization, which is not noted on the outside surfaces of the same samples. We suggest that the intense corrosion is due to the original content of the vessels, significantly affecting the glass over a short period of time.

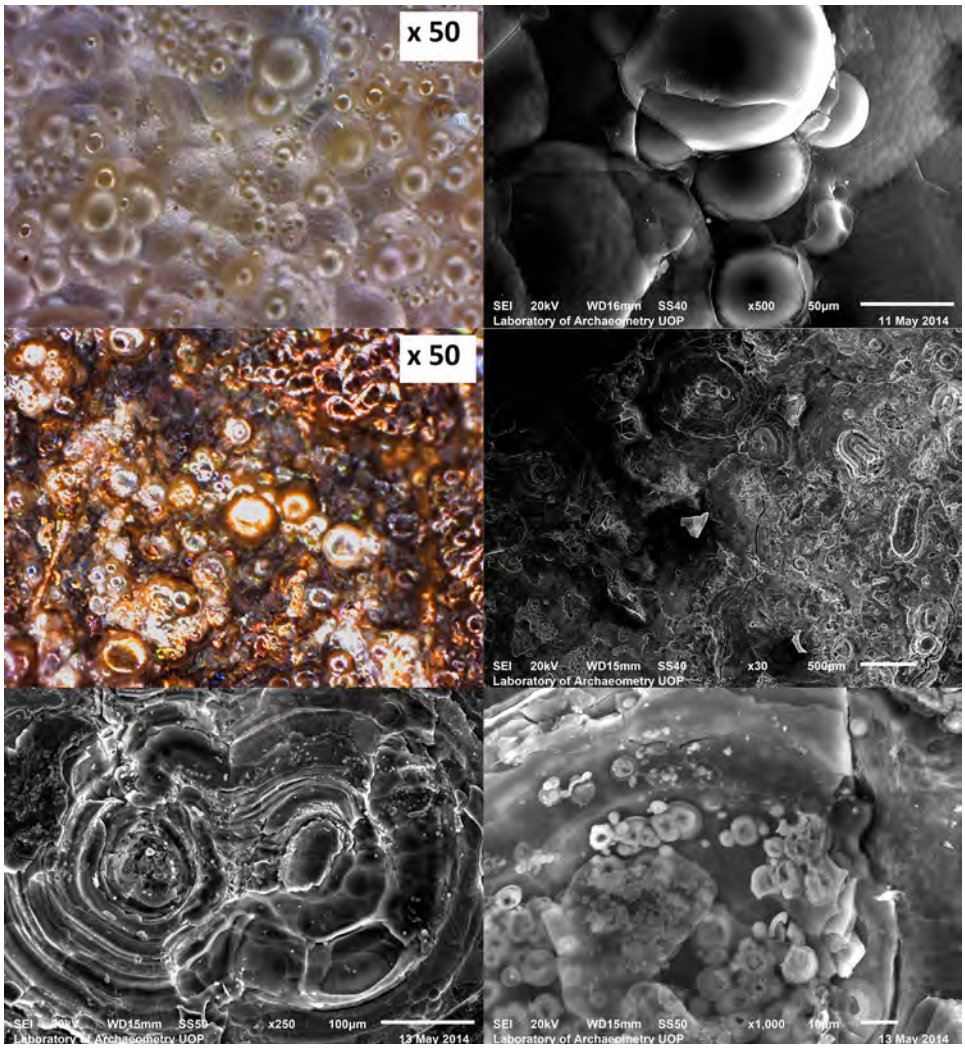

Figure 8 FOM and SEM images of the iridescent (up) and the browning layer (middle and down) of the plant-ash sample.

Table 5 EDS compositional analysis of the iridescent and the browning corrosion layer (weight %, normalised to 100%).

	Na_2O	MgO	Al_2O_3	P2O5	SiO_2	K_2O	CaO	TiO_2	MnO	FeO	PbO
Pristine glass	20.21	4.23	2.08	63.59	1.20	0.72	1.33	5.05	0.78	0.80	n.d.
Iridescent layer	n.d.	n.d.	11.67	n.d.	81.10	n.d.	5.52	n.d.	n.d.	n.d.	n.d.
Browning layer	n.d.	n.d.	6.02	n.d.	59.04	n.d.	6.56	1.39	14.65	9.35	1.73

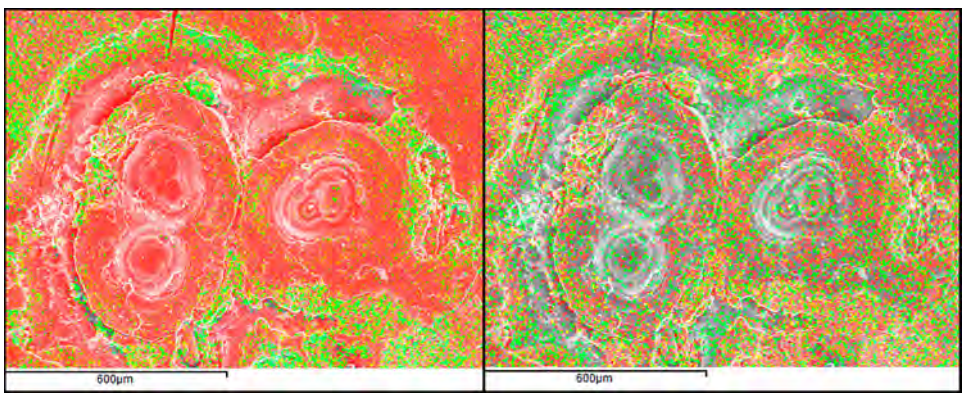

Figure 9 Mapping of the concentration of Si, Mn and Fe on a biocorrosion formation on the browning layer. Left image: Red spots: Si; Yellow spots: Mn. Right image: Red spots: Mn; Yellow spots: Fe.

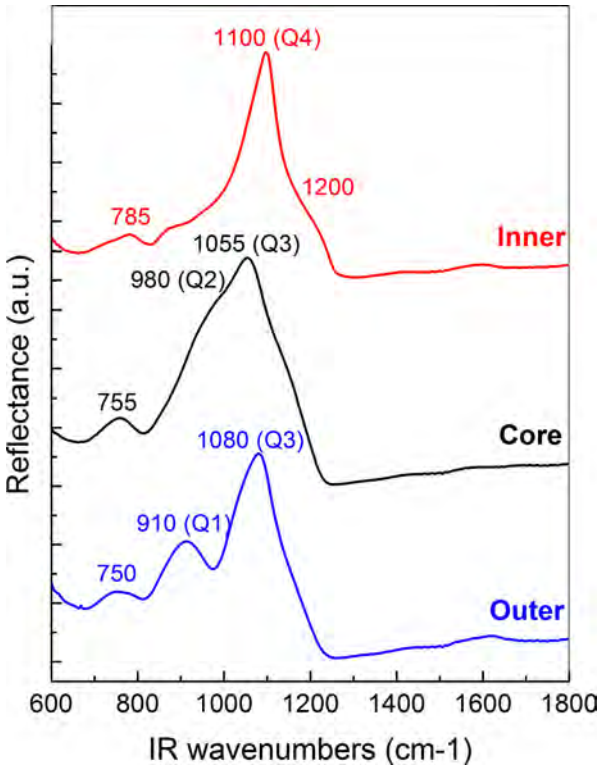

Figure 10 IR spectra of the core, the outside and the inside surface of the walls of a glass vessel.

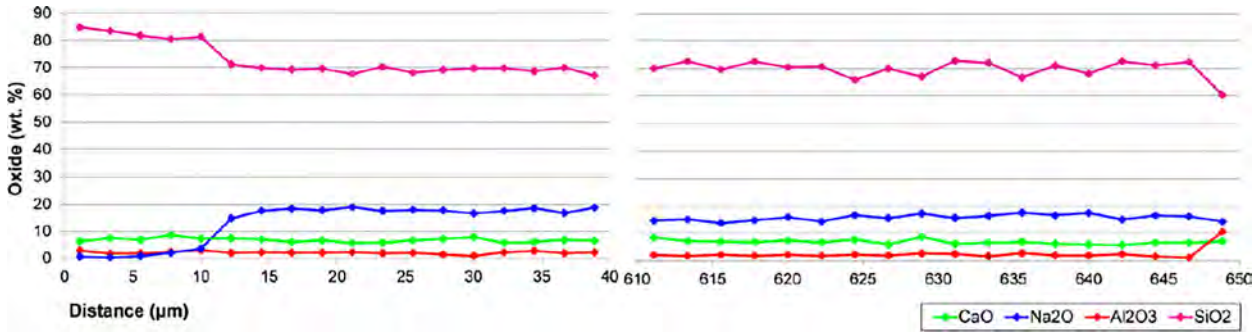

Figure 11 Concentration profile by SEM/EDS (0 μm: Inside surface; 650 μm: Outside surface).

Taking the above mentioned patterns into consideration, it is evident that samples of very similar concentration, found buried together, show significantly different degrees and mechanisms of corrosion. The complexity of the corrosion effects noted highlights the need for further research on the corrosion of archaeological glass.

Acknowledgements

EP gratefully acknowledges financial support from the PELOPS Scholarship Program of the University of the Peloponnese. The authors acknowledge permits granted by the Greek Ministry of Culture to enable the study of the assemblage.

References

Archaiologikon Deltion. (In press), *Chronika 2013* (in Greek).

Bertoncello, R., L. Milanese, U. Russo, D. Pedron, P. Guerriero, and S. Barison. 2002. "Chemistry of cultural glasses: the early medieval glasses of Monselice's hill (Padova, Italy)." *Journal of Non-Crystalline Solids* 306: 249–262.

Doménech-Carbó, M.-T., A. Doménech-Carbó, L. Osete-Cortina, and M.C. Saurí-Peris. 2006. "A study on corrosion processes of archaeological glass from the Valencian region (Spain) and its consolidation treatment." *Microchimica Acta* 154: 123–142.

Eastaugh, N., V. Walsh, T. Chaplin, and R. Siddall R, ed/s. 2004. *The pigment Compendium, A dictionary of historical pigments*. Oxford: Elsevier.

Ganio, M., S. Boyen, T. Fenn, R. Scott, S. Vanhoutte, D. Gimeno, and P. Degryse. 2012. "Roman glass across the Empire: an elemental and isotopic characterization." *Journal of Analytical Atomic Spectrometry* 27: 743–753.

Gallo, F., A. Silvestri, and G. Molin. 2013. "Glass from the Archaeological Museum of Adria (North-East Italy): new insights into Early Roman production technologies." *Journal of Archaeological Science* 40: 2589–2605.

Gedzevičiūtė, V., N. Welter, U. Schüssler, and C. Weiss. 2009. "Chemical composition and colouring agents of Roman mosaic and millefiori glass, studied by electron microprobe analysis and Raman microspectroscopy." *Archaeological and Anthropological Sciences* 1: 15–29.

Hottentot, W., and S.M.E Van Lith. 2006. "Römische Schönheitspflegemittel in Kugeln und Vögeln aus Glas." *Bull. Antieke Beschaving* 81: 185–198.

Jackson, C.M. 2005. "Making colourless glass in the Roman period." *Archaeometry* 47 (4): 763–780.

Jackson, C.M., and S. Cottam. 2015. "'A green thought in a green shade'; Compositional and typological observations concerning the production of emerald green glass vessels in the 1st century A.D." *Journal of Archaeological Science* 61: 139–148.

Kolonas, L. 2002. "Glass vessels from Patras." In: *Glass-From Antiquity until today*. Athens: Society of Messenian Archaeological Studies (in Greek).

Liritzis, I., C. Salter, and H. Hatcher. 1997. "Chemical composition of some Greco-Roman glass fragments from Patras, Greece." *European Journal of PACT* 45 (I2): 25–34.

Liritzis, I., and N. Zacharias. 2011. "Portable XRF of archaeological artifacts: Current research, potentials and limitations." In: *X-Ray fluorescence spectrometry (XRF) in geoarchaeology*, eds. Shackley M.S. New York: Springer.

Lynch, M.E., D.C. Folz, and D.E. Clark. 2007. "Use of FTIR reflectance spectroscopy to monitor corrosion mechanisms on glass surfaces." *Journal of Non-Crystalline Solids* 353: 2667–2764.

Mirti, P., A. Casoli, and L. Appolonia. 1993. "Scientific analysis of Roman glass from Augusta Praetoria." *Archaeometry* 35 (2): 225–240.

Mirti, P., M. Pace, M.M. Negro Ponzi, and M. Aceto. 2008. "ICP-MS analysis of glass fragments of Parthian and Sasanian epoch from Seleucia and Veh Ardašīr (central Iraq)." *Archaeometry* 50 (3): 429–450.

Möncke, D., D. Palles, N. Zacharias, M. Kaparou, E.I. Kamitsos, and L. Wondraczek. 2013. "Formation of an outer borosilicate glass layer on Late Bronze Age Mycenaean blue vitreous relief fragments." *Physics and Chemistry of Glasses: European Journal of Glass Science and Technology* (Part B) 54: 52–59.

Papageorgiou, M. 2014. "Archaeological and archaeometric analysis of glass artefacts of the Late Antiquity from western Peloponnese" unpublished PhD thesis, National and Kapodistrian University of Athens (in Greek).

Paynter, S. 2006. " Analyses of colourless Roman glass from Binchester, County Durham." *Journal of Archaeological Science* 3: 1037–1057.

Paynter, S., and D. Dungworth. 2011. *Archaeological evidence for glass-working. Guidelines for best practice*. Swindon, English Heritage.

Pérez-Arantegui, J., E. Ribechini, G. Cepriá, I. Degano, M.P. Colombini, J. Paz-Peralta, and E. Ortiz-Palomar. 2009. "Colorants and oils in Roman make-ups – an eye witness account." *Trends in Analytical Chemistry* 28 (8): 1019–1028.

Perez Y Jorba, M., J.P. Dallas, C. Bauer, C. Bahezre, and J.C. Martin. 1980. "Deterioration of stained glass by atmospheric corrosion and microorganisms." *Journal of Materials Science* 15: 1640–1647.

Sayre, E.V., and R.W. Smith. 1961. "Compositional categories of ancient glass." *Science* 133: 1824–6.

Silvestri, A., G. Molin, and G. Salviulo. 2005. "Roman and Medieval glass from the Italian area: Bulk characterization and relationships with production technologies." *Archaeometry* 47 (4): 797–816.

Tournié, A., P. Ricciardi, and Ph. Colomban. 2008. "Glass corrosion mechanisms: A multiscale analysis." *Solid State Ionics* 179: 2142–2154.

Triantafyllidis, P. 2006. "Preroman and Roman glassmaking and glass-working in Greece." *Proceedings of the 2nd International Conference of Ancient Greek Technology*, Athens (in Greek).

Triantafyllidis, P. 2007. "Glassmakers of Late Antiquity in Greece: Philological References and New Archaeological Evidence." *Journal of Glass Studies* 49: 262–264.

Van der Linder, V., P. Cosyns, O. Schalm, S. Cagno, K. Nys, K. Janssens, A. Nowak, B. Wagner, and E. Bulska. 2009. "Deeply coloured and black glass in the Northern provinces of the Roman Empire: Differences and similarities in chemical composition before and after AD 150." *Archaeometry* 51 (5): 822–844.

Van Elslande, E., V. Guérineau, V. Thirioux, G. Richard, P. Richardin, O. Laprévote, G. Hussler, and P. Walter. 2008. "Analysis of ancient Greco–Roman cosmetic materials using laser desorption ionization and electrospray ionization mass spectrometry." *Analytical and Bioanalytical Chemistry* 390: 1873–1879.

Zacharias N., K. Beltsios, A. Oikonomou, A.G. Karydas, Y. Bassiakos, C.T. Michael, and Ch. Zarkadas. 2008. "Solid-state luminescence for the optical examination of archaeological glass beads." *Optical Materials* 30: 1127–1133.

Zacharias, N., and E. Palamara. 2016. "Chapter 12: Glass Corrosion: Issues and Approaches for Archaeological Science." In: *Recent Advances in the the Scientific Research on Ancient Glass and Glasses*, eds. Fuxi, G., Qinghui, L. and Henderson, J., 233–248. Singapore: World Scientific.